Antiferromagnetic fluctuations and dominant d_{xy}-wave pairing symmetry in nickelate-based superconductors

Chao Chen [●],[1] Runyu Ma [●],[1] XueLei Sui,[2] Ying Liang,[1] Bing Huang,[2,1] and Tianxing Ma [●][1,2,*]

[1]*Department of Physics, Beijing Normal University, Beijing 100875, China*
[2]*Beijing Computational Science Research Center, Beijing 100084, China*

Motivated by recent experimental studies on superconductivity found in nickelate-based materials, we study the temperature dependence of the spin correlation and the superconducting pairing interaction within an effective two-band Hubbard model by the quantum Monte Carlo method. Based on parameters extracted from first-principles calculations, our intensive numerical results reveal that the pairing with a d_{xy}-wave symmetry firmly dominates over other pairings at low temperature, which is mainly determined by the Ni $3d$ orbital. It is also found that the effective pairing interaction is enhanced as the on-site interaction increases, demonstrating that the superconductivity is driven by strong electron-electron correlation. Even though the (π, π) antiferromagnetic correlation could be enhanced by electronic interaction, there is no evidence for long-range antiferromagnetic order exhibited in nickelate-based superconductors. Moreover, our results offer possible evidence that the pure electron correlation may not account for the charge density wave state observed in nickelates.

I. INTRODUCTION

Understanding the mechanism of high-T_c superconductivity [1–7] and intertwining symmetry-breaking orders [8–10] has always been a central issue in condensed matter physics. Recently, the discovery of superconductivity in the family of Sr-doped RNiO$_2$ (R = Nd, La, Pr) [11–15] has attracted great research interest, which may provide a new opportunity for further understanding unconventional superconductivity [16–25]. Among them, one essential object is to identify the dominant superconducting pairing form, which remains a major challenge of today's studies on this family. In a single-particle tunneling experiment on a Sr-doped NdNiO$_2$ film surface, researchers detected singlet pairing, but they could not distinguish whether it is an s wave, d wave, or their mixture [26]. At present, some theoretical studies of nickelate-based superconductors have been based on models with one-orbital (Ni $3d$) band structures that support these materials being captured by a one-band Hubbard model [27–29], and they have revealed a dominant d-wave pairing in their model [27,28]. However, others have proposed various possibilities for multiband models [30–35]. The t-J-K model, which considers the Kondo coupling, exhibits a transition between the d wave and $(d + is)$ wave of the dominant pairing at large hole doping [36]. Research on the controversial pair symmetry of nickelates is necessary both experimentally and theoretically. From the theoretical viewpoint, using unbiased numerical techniques is believed to be the only opportunity to achieve this goal if the electronic correlation dominates in the system.

Besides the superconductivity, the spin density wave (SDW) [37–39] and charge density wave (CDW) [40–45], which are observed in nickelates, also attract high attention in quest of their origins. Previous theoretical works on density functional theory (DFT) [46–50] have systematically studied the characteristics of nickelate electronic structures. It is found that there are both similarities and differences compared with those of cuprates [31,33,48–53]. These results provide a cornerstone to study the magnetism, superconductivity, and CDW in the nickelate family. According to the DFT calculation of RNiO$_2$ [48–50], the two bands near E_F mainly contributed to its physical properties. One band, composed of Ni $3d_{x^2-y^2}$ and O $2p$ orbitals, has a Zhang-Rice-singlet-like character, while the contribution of oxygen in the nickelates is smaller than that in cuprates, and the other band, composed of the R $5d$ orbital, forms an important metallic electron pocket. These two orbitals hybridize, forming a two-band system, where the strongly correlated Ni layers play an important role [48–50].

To identify the superconducting pairing form of nickelate-based materials, we perform a quantum Monte Carlo study of the spin correlation and superconducting pairing interaction in an effective two-band microscopic model based on parameters extracted from first-principles calculations. From the results of the Wannier orbitals [48,50], a two-band model is constructed that contains two main bands near E_F, and this model also contains interorbital coupling between the Ni $3d$ orbital and the R $5d$ orbital. The calculations of the pairing correlation show that there exists an extensive d-wave channel that firmly dominates over other pairings at low temperature and the pairing channel is determined by the Ni $3d$ orbital. For different fillings $\langle n \rangle$ = 1.0, 0.9, and 0.8, the (π, π) antiferromagnetic (AFM) correlation and the effective pairing interaction are both enhanced as the on-site

interaction increases. Our unbiased calculations demonstrate that the superconductivity and AFM correlation in nickelate-based superconductors should be driven by electron-electron correlation. Although the (π, π) antiferromagnetic correlation could be enhanced by electronic interaction, there is no evidence for long-range antiferromagnetic order exhibited in nickelate-based superconductors. Additionally, by considering the nearest-neighbor repulsion of the Ni 3d orbital, the CDW state exhibits a $q = (\pi, \pi)$ pattern.

II. MODEL AND METHODS

In the two-band Hubbard model, the tight-binding part contains intralayer hopping, interlayer hopping, and the strongly correlated Ni layer. Therefore, the nickel-square lattice Hamiltonian can be written as

$$H = H_1 + H_2 + H_3 + H_4,$$

$$H_1 = t_3^{\text{Nd-Ni}} \sum_{\mathbf{i}\eta\sigma} [a_{\mathbf{i}\sigma}^\dagger b_{\mathbf{i}+\eta\sigma} + \text{H.c.}],$$

$$H_2 = t_1^{\text{Nd}} \left[\sum_{\mathbf{i}\tau_1\sigma} a_{\mathbf{i}\sigma}^\dagger a_{\mathbf{i}+\tau_1\sigma} \right] + t_2^{\text{Nd}} \left[\sum_{\mathbf{i}\tau_2\sigma} a_{\mathbf{i}\sigma}^\dagger a_{\mathbf{i}+\tau_2\sigma} \right]$$

$$+ t_3^{\text{Nd}} \left[\sum_{\mathbf{i}\tau_3\sigma} a_{\mathbf{i}\sigma}^\dagger a_{\mathbf{i}+\tau_3\sigma} \right],$$

$$H_3 = t_1^{\text{Ni}} \left[\sum_{\mathbf{i}\tau_1\sigma} b_{\mathbf{i}\sigma}^\dagger b_{\mathbf{i}+\tau_1\sigma} \right] + t_2^{\text{Ni}} \left[\sum_{\mathbf{i}\tau_2\sigma} b_{\mathbf{i}\sigma}^\dagger b_{\mathbf{i}+\tau_2\sigma} \right]$$

$$+ t_3^{\text{Ni}} \left[\sum_{\mathbf{i}\tau_3\sigma} b_{\mathbf{i}\sigma}^\dagger b_{\mathbf{i}+\tau_3\sigma} \right],$$

$$H_4 = U \sum_{\mathbf{i}} n_{b\mathbf{i}\uparrow} n_{b\mathbf{i}\downarrow} + \mu \sum_{\mathbf{i}\sigma} [(1 + \Delta/\mu) n_{a\mathbf{i}\sigma} + n_{b\mathbf{i}\sigma}]. \quad (1)$$

Here, $a_{\mathbf{i}\sigma}$ ($a_{\mathbf{i}\sigma}^\dagger$) annihilates (creates) electrons at site $\mathbf{R_i}$ with spin σ ($\sigma = \uparrow, \downarrow$) on sublattice A, $b_{\mathbf{i}\sigma}$ ($b_{\mathbf{i}\sigma}^\dagger$) annihilates (creates) electrons at site $\mathbf{R_i}$ with spin σ ($\sigma = \uparrow, \downarrow$) on sublattice B, $n_{a\mathbf{i}\sigma} = a_{\mathbf{i}\sigma}^\dagger a_{\mathbf{i}\sigma}$, $n_{b\mathbf{i}\sigma} = b_{\mathbf{i}\sigma}^\dagger b_{\mathbf{i}\sigma}$, $\eta = (\pm 3\hat{x}, \pm 3\hat{y})$, $\tau_1 = (\pm 2\hat{x}, 0)$ and $(0, \pm 2\hat{y})$, $\tau_2 = (\pm 2\hat{x}, \pm 2\hat{y})$, and $\tau_3 = (\pm 4\hat{x}, 0)$ and $(0, \pm 4\hat{y})$. Our first-principles calculations give consistent on-site energy and hopping parameters with previous works [48–50]. For more details about our Wannier downfolding of NdNiO$_2$, please see Table II in the Appendix. For simplicity and clarity, we mainly take the parameters from Refs. [48–50] and list the hopping parameters of NdNiO$_2$ that we use in Table I at $k_z = 0, \pi/2$ and π. From the analysis of the first-principles calculations [48–50,54,55], $\Delta = \Delta_1 - \Delta_2$ represents the on-site energy difference between the Nd 5d orbital and the Ni 3d orbital. In the following calculations, we mainly discuss the cases of $k_z = 0$ and $k_z = \pi$.

Our simulations are mainly performed on the lattice shown in Fig. 1(a) of $L = 8$ (the total number of lattice sites is $N_s = 2 \times L^2 = 128$) by using the determinant quantum Monte Carlo (DQMC) method at finite temperature with periodic boundary conditions. The basic strategy of the DQMC method is to express the partition function as high-dimensional integrals on a set of random auxiliary fields. Then, the Monte

TABLE I. Hopping parameters (in units of eV) for the tight binding model from Refs. [48–50].

t	$k_z = 0$	$k_z = \pi/2$	$k_z = \pi$
		t^{Nd}	
Δ_1	0.633	1.305	1.287
t_1	−0.380	−0.028	0.444
t_2	0.084	−0.090	−0.180
t_3	0.003	0.027	0.051
		t^{Ni}	
Δ_2	0.242	0.308	0.374
t_1	−0.374	−0.374	−0.374
t_2	0.094	0.094	0.094
t_3	−0.043	−0.043	−0.043
		$t^{\text{Nd-Ni}}$	
t_3	0.020	0.020	0.020

Carlo techniques complete the integral. In the simulations, we use 3000 sweeps to equilibrate the system and an additional 10 000–40 000 sweeps to generate measurements. These measurements were split into 10 bins and provided the basis of coarse-grain averages. The errors were calculated based on the standard deviation from the average. For more technical details, please see Refs. [56–59], as well as information in the Appendix.

As magnetic excitation possibly plays a significant role in the superconductivity mechanism of electronic correlated systems, we investigate the spin susceptibility in the z direction at zero frequency,

$$\chi(q) = \int_0^\beta d\tau \sum_{d,d'=a,b} \sum_{\mathbf{i},\mathbf{j}} e^{iq\cdot(\mathbf{i}_d - \mathbf{j}_{d'})} \langle m_{\mathbf{i}_d}(\tau) \cdot m_{\mathbf{j}_{d'}}(0) \rangle, \quad (2)$$

where $m_{\mathbf{i}_a}(\tau) = e^{H\tau} m_{\mathbf{i}_a}(0) e^{-H\tau}$ with $m_{\mathbf{i}_a} = a_{\mathbf{i}\uparrow}^\dagger a_{\mathbf{i}\uparrow} - a_{\mathbf{i}\downarrow}^\dagger a_{\mathbf{i}\downarrow}$ and $m_{\mathbf{i}_b} = b_{\mathbf{i}\uparrow}^\dagger b_{\mathbf{i}\uparrow} - b_{\mathbf{i}\downarrow}^\dagger b_{\mathbf{i}\downarrow}$. To study the superconducting property of nickelate-based superconductors, we calculated the pairing susceptibility,

$$P_\alpha = \frac{1}{N_s} \sum_{\mathbf{i},\mathbf{j}} \int_0^\beta d\tau \langle \Delta_\alpha^\dagger(\mathbf{i}, \tau) \Delta_\alpha(\mathbf{j}, 0) \rangle, \quad (3)$$
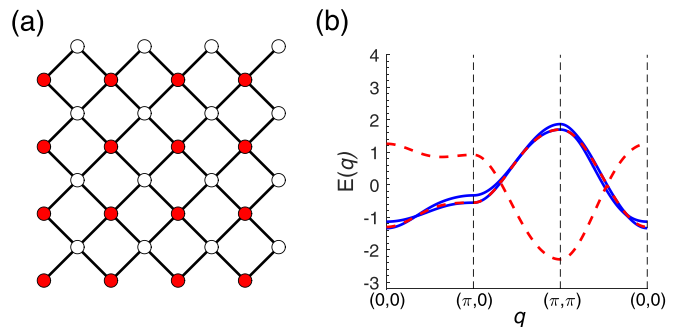

FIG. 1. (a) Here, red and white circles indicate different sublattices, A and B. The nearest distance between B and B (or A and A) is 2. (b) The energy band along the high-symmetry line in the unfolded Brillouin zone. Solid blue lines: $k_z = 0$; dashed red lines: $k_z = \pi$ in Table I.
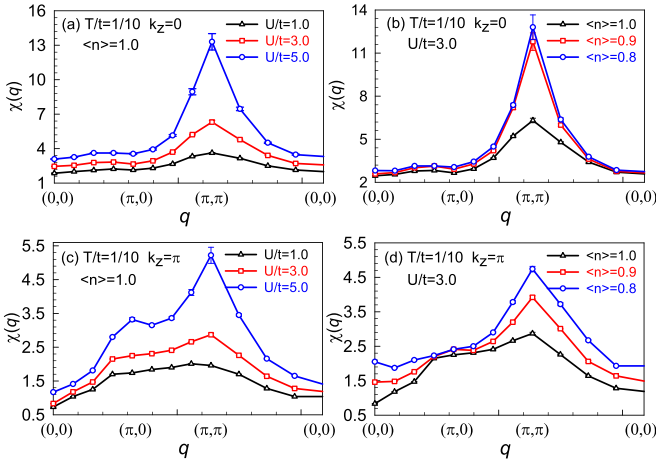
FIG. 2. Magnetic susceptibility $\chi(q)$ versus momentum q, (a) for different U at $\langle n \rangle = 1.0$, (b) for different fillings at $U/t = 3.0$ (where $t = |t_1^{Ni}| = 0.374$ eV) and $k_z = 0$ on a 2×8^2 lattice, (c) for different U at $\langle n \rangle = 1.0$, (d) for different fillings at $U/t = 3.0$ and $k_z = \pi$ on a 2×8^2 lattice.

where α denotes the pairing symmetry. Due to the constraint of different on-site Hubbard interaction in two sublattices, pairing between the same sublattices is favored, and the corresponding order parameter $\Delta_\alpha^\dagger(\mathbf{i})$ is written as

$$\Delta_\alpha^\dagger(\mathbf{i}) = \sum_l f_\alpha^\dagger(\delta_l)(a_{\mathbf{i}\uparrow} b_{\mathbf{i}+\delta_l\downarrow} - a_{\mathbf{i}\downarrow} b_{\mathbf{i}+\delta_l\uparrow})^\dagger,$$

where $f_\alpha(\delta_{\mathbf{l}})$ stands for the form factor of the pairing function. The vectors $\delta_{\mathbf{l}}$ ($l = 1, 2, 3, 4$) represent the nearest inter-sublattice connections, where δ is ($\pm\hat{x}, \pm\hat{y}$), or the nearest intrasublattice connections where δ' is ($\pm2\hat{x}, 0$) and $(0, \pm2\hat{y})$.

Furthermore, in order to explore the CDW state, we define the density-density correlation function [60–62],

$$C(R) = \frac{1}{N_s N_R} \sum_{\mathbf{i}} \sum_{|\mathbf{j}-\mathbf{i}|=\mathbf{R}} \langle (n_i - \langle n_i \rangle)(n_j - \langle n_j \rangle) \rangle. \quad (4)$$

Here, n_i and n_j denote the electronic number operator at sites $\mathbf{R_i}$ and $\mathbf{R_j}$. R is the distance between site i and site j. The N_R is the total number of distance R. And its Fourier transform can be written as

$$C(q) = \frac{1}{N_s} \sum_{\mathbf{R}} e^{iqR} C(R). \quad (5)$$

III. RESULTS AND DISCUSSION

To study the magnetic correlations, we calculated the spin susceptibility $\chi(\mathbf{q})$ in Fig. 2 at different U and fillings $\langle n \rangle$ at temperature $T/t = 1/10$. In Fig. 2, one can notice that there is a sharp peak at (π, π), which indicates the domination of AFM correlation at both $k_z = 0$ and $k_z = \pi$. In Figs. 2(a) and 2(c), we can see that the AFM correlation is enhanced as U increases, which indicates that such an AFM correlation is driven by strong electron-electron correlation. Figures 2(b) and 2(d) show that the peak is enhanced at fillings $\langle n \rangle = 0.9$ and 0.8, which indicates that the AFM correlation is promoted when the system is doped away from half filling. Recently, resonant inelastic x-ray scattering experiments have revealed
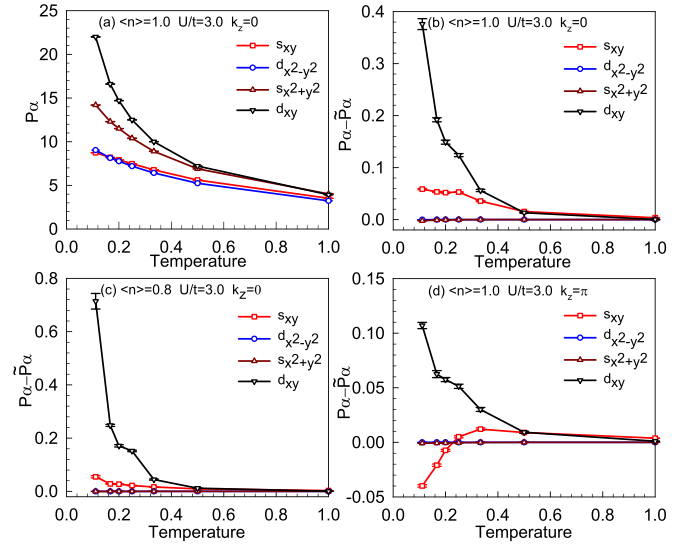

FIG. 3. (a) Pairing susceptibility P_α and (b) the effective pairing interaction P_α-$\tilde{P}_\alpha$ as a function of temperature for different pairing symmetries at $\langle n \rangle = 1.0$, $U/t = 3.0$, and $k_z = 0$ on a 2×8^2 lattice. (c) The effective pairing interaction P_α-$\tilde{P}_\alpha$ as a function of temperature for different pairing symmetries at $\langle n \rangle = 0.8$, $U/t = 3.0$, and $k_z = 0$ on a 2×8^2 lattice, (d) at $\langle n \rangle = 1.0$, $U/t = 3.0$, and $k_z = \pi$ on a 2×8^2 lattice.

an AFM exchange interaction [38]. Our results here might provide evidence for the AFM exchange couplings observed in infinite-layer nickelates.

In Fig. 3(a), we show the temperature dependence of the pairing susceptibilities for different pairing symmetries at half filling with $U/t = 3.0$ at $k_z = 0$. We can clearly observe that the pairing susceptibilities for various pairing symmetries increase with decreasing temperature. Most strikingly, d_{xy} increases much faster than any other pairing symmetry as the temperature is lowered. This indicates that the d_{xy} pairing symmetry is dominant over the other pairing symmetry at half filling. Our further results also illustrate that the d_{xy} pairing symmetry is robust at different fillings and U.

The effective pairing interaction is a direct probe for the superconductivity. To extract the effective pairing interaction, the uncorrelated single-particle contribution $\tilde{P}_\alpha(\mathbf{i}, \mathbf{j})$ is calculated, which is achieved by replacing $\langle a_{\mathbf{i}\downarrow}^\dagger b_{\mathbf{j}\uparrow} a_{\mathbf{i}+\delta_l\downarrow}^\dagger b_{\mathbf{j}+\delta_{l'}\uparrow} \rangle$ in Eq. (3) with $\langle a_{\mathbf{i}\downarrow}^\dagger b_{\mathbf{j}\uparrow} \rangle \langle a_{\mathbf{i}+\delta_l\downarrow}^\dagger b_{\mathbf{j}+\delta_{l'}\uparrow} \rangle$, and then we get the effective pairing interaction P_α-$\widetilde{P}_\alpha$. In Figs. 3(b) and 3(c), it is obvious that P_α-$\tilde{P}_\alpha$ presents a very similar temperature dependence to that of P_α at $\langle n \rangle = 1.0$ or $\langle n \rangle = 0.8$. Moreover, the effective pairing interaction for d_{xy} pairing is always positive and increases much faster than any other pairing symmetry at low temperatures. Such a temperature dependence shows that there indeed exists attraction for the d_{xy} pairing at $k_z = 0$. From Fig. 3(d), we can find that the d_{xy} pairing symmetry is also dominant at $k_z = \pi$. Therefore, although hopping parameters t_i^{Nd} and the on-site energy difference Δ are changed at different k_z, the investigated magnetism and pairing interaction show identical physical results. In the following, we mainly discuss hopping parameters at $k_z = 0$ for simplicity.
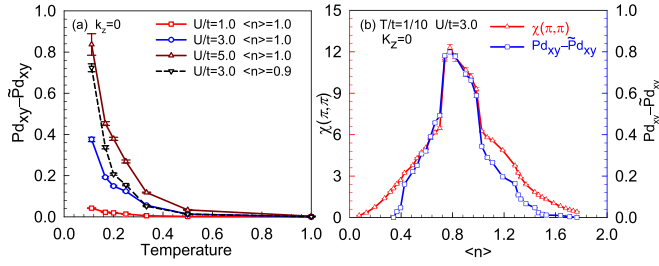
FIG. 4. (a) The effective pairing interaction $P_{d_{xy}}$-$\tilde{P}_{d_{xy}}$ as a function of temperature for different U at $\langle n \rangle = 1.0$ and $k_z = 0$ on a 2×8^2 lattice. (b) The effective pairing interaction $P_{d_{xy}}$-$\tilde{P}_{d_{xy}}$ and the (π, π) AFM correlation $\chi(\pi, \pi)$ as a function of fillings at $T/t = 1/10$, $U/t = 3.0$, and $k_z = 0$ on a 2×8^2 lattice.

Figure 4(a) shows the effective pairing interaction as a function of temperature for the d_{xy} wave at different U. We can see that the effective pairing interaction of the d_{xy} wave is enhanced with increasing U. For $U/t = 1.0$, the effective pairing interaction $P_{d_{xy}}$-$\tilde{P}_{d_{xy}}$ is very small even in the low-temperature region, which may be due to the small AFM structure of the system in Fig. 2(a). For $U/t = 3.0$ and $U/t = 5.0$, remarkably, the effective pairing interaction $P_{d_{xy}}$-$\tilde{P}_{d_{xy}}$ tends to diverge at low temperatures, and with increasing U, this divergence tends to be promoted. This indicates that the d_{xy} pairing superconductivity should be driven by a strong electron-electron correlation. In Fig. 4(b), we studied the filling dependence of the effective pairing interaction $P_{d_{xy}}$-$\tilde{P}_{d_{xy}}$ and the (π, π) AFM correlation $\chi(\pi, \pi)$ at $T/t = 1/10$, $U/t = 3.0$, and $k_z = 0$. Figure 4(b) indicates that the optimal electron filling is slightly below $\langle n \rangle = 0.8$, where the effective pairing interaction and the AFM correlation is largest. Figures 2 and 4 show that the increase in the peak at (π, π) of spin susceptibility is correlated with the promotion of the pairing susceptibility. This directly confirms that the (π, π) AFM fluctuations enhance the d_{xy} pairing.

From the above studies, we know that the system exhibits local antiferromagnetism. To further explore whether there is a long-range AFM order, we also calculate the AFM spin structure factor,

$$S_{\text{AFM}} = \frac{1}{N_s} \left\langle \left[\sum_r (-1)^r \hat{S}_{br}^z \right]^2 \right\rangle. \qquad (6)$$

Here, $\hat{S}_{br}^z$ is the z component spin operator on the B sublattice. When $\lim_{N_s \to \infty}(S_{\text{AFM}}/N_s) > 0$, it indicates the onset of long-range AFM order. In Fig. 5(a), we present the results of the AFM spin structure factors as a function of β for different interaction strengths U and lattice sizes L, which demonstrates the spin structure factor is nearly saturated at $\beta = 10$. Interesting, S_{AFM} decreases as the lattice size increases at low temperatures, which indicates that there is no long-range AFM order at $U/t \leqslant 5.0$ and $\langle n \rangle = 1.0$. In Figs. 5(b) and 5(c), it is shown that $\chi(q)$ has a very minor size dependency with lattice sizes $L = 10$ and 12 at $\langle n \rangle = 1.0$ or $\langle n \rangle = 0.8$. Actually, it is more difficult to exhibit long-range AFM order at $\langle n \rangle = 0.8$, since $\chi(q)$ decreases as the lattice size increases from $L = 8$ to 10. Different from the AFM spin structure factors, as that shown in Fig. 5(d), the effective pairing interaction increases
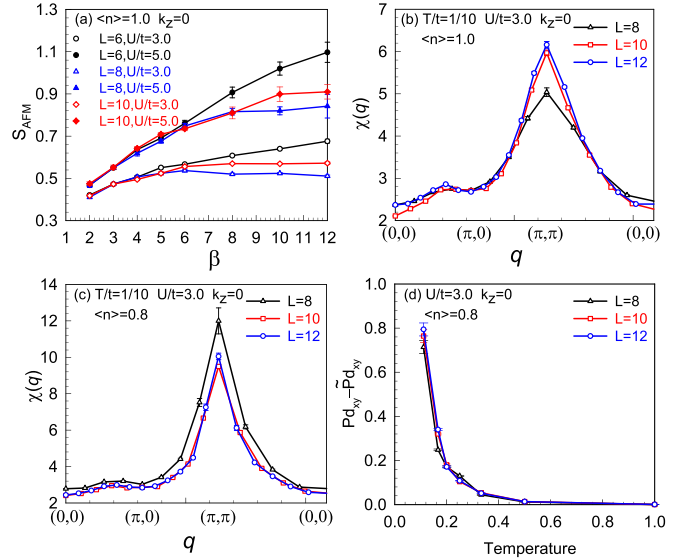

FIG. 5. (a) The AFM spin structure factor S_{AFM} depends on $\beta = 1/T$ with different interaction strengths and lattice sizes at $\langle n \rangle = 1.0$ and $k_z = 0$. (b) Magnetic susceptibility $\chi(q)$ versus momentum q for different lattice sizes at $U/t = 3.0$, $T/t = 1/10$, $k_z = 0$ for $\langle n \rangle = 1.0$ and (c) $\langle n \rangle = 0.8$. (d) The effective pairing interaction $P_{d_{xy}}$-$\tilde{P}_{d_{xy}}$ as a function of temperature for different lattice sizes at $\langle n \rangle = 0.8$, $U/t = 3.0$, and $k_z = 0$.

very fast as the temperature decreases, and has a potential to diverge as the temperature is low enough. Moreover, $P_{d_{xy}}$-$\tilde{P}_{d_{xy}}$ increases slightly as the system size increases. These two facts, different from the magnetic order, indicate that the superconducting order with d_{xy} symmetry should survive even at thermodynamic limit. Therefore, our numerical results reveal that the d_{xy}-wave symmetry firmly dominates over other pairings and the system may exhibit superconductivity as the temperature is low enough. Two closely related theoretical works by DMFT also report the absence of long-range AFM order and its competition with superconductivity [63,64].

At last, to discuss the electron correlation effect on the CDW state, we consider the nearest-neighbor repulsion of the Ni $3d$ orbital in the Hamiltonian, which can be written as

$$H_V = V \sum_{\mathbf{i}, \tau_1} n_{b\mathbf{i}} n_{b(\mathbf{i}+\tau_1)}. \qquad (7)$$

In Fig. 6(a), we can notice the density-density correlation function $C(R)$ develops a staggered pattern as the interaction strength increases to $V = 0.9t$, which indicates the onset of the CDW. Figure 6(b) shows that the peak of $q = (\pi, \pi)$ is quickly enhanced at $V = 0.9t$, which also is a signal of the CDW's presence. Due to the serious sign problem at low temperature or high interaction, we only display the temperature effect at $T/t = 1/4, 1/5, 1/6$, and $V = 0.9t$ in the inset of Fig. 6(b) and can see a small enhancement of charge correlations with decreasing temperature.

IV. SUMMARY

In summary, within an effective two-band model for nickelate-based superconductors, we study the spin correlation, the superconducting pairing interaction, and the
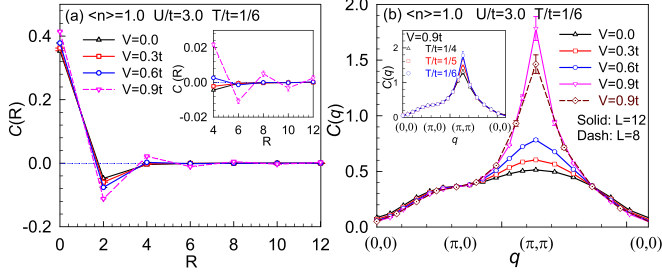
FIG. 6. (a) The density-density correlations $C(R)$ of Ni $3d$ orbital as a function of distance R for different V at $\langle n \rangle = 1.0$, $U/t = 3.0$, and temperature $T/t = 1/6$ on a 2×12^2 lattice. Inset: The enlarged $C(R)$ for $R \geqslant 4.0$. (b) The density-density correlations $C(q)$ versus momentum q for different V at $\langle n \rangle = 1.0$, $U/t = 3.0$, and $T/t = 1/6$ on a 2×12^2 or 2×8^2 lattice. Inset: $C(q)$ versus momentum q for different T at $\langle n \rangle = 1.0$, $U/t = 3.0$, and $V/t = 0.9$ on a 2×12^2 lattice.

density-density correlation by using the unbiased numerical techniques of DQMC. We identify that the d_{xy} wave pairing channel is dominant in nickelate-based superconductors, which might support the recent London penetration depth experiment [65]. Both the (π, π) AFM and the pairings with the d_{xy} symmetry are enhanced with increasing electron-electron correlation, especially in the low-temperature region. Moreover, as the system is doped away from half filling, the effective pairing interaction of d_{xy} symmetry is also enhanced and reaches maximum at $\langle n \rangle \approx 0.8$. Our results also indicate that the system may not exhibit long-range AFM, which is also not observed experimentally [37–39,66]. Although the study of charge correlations does not display a wave vector $q \approx (0.333, 0)$, which has been observed in experiments [41,42], this initial attempt reveals a more complex mechanism should be established to illustrate the CDW phase in nickelates [67]. In a further work, we simulate the effect of symmetry breaking by modifying the periodic chemical potential, which shows a different CDW pattern [68]. All in all, our work shares exact numerical results to understand the superconducting and symmetry-breaking orders of nickelate-based materials.

APPENDIX

In this Appendix, we present detailed information on hopping parameters for our Wannier downfolding, the pairing symmetries of the nickel square, correction of the Trotter error, and the sign problem.

TABLE II. On-site energy and hopping parameters (eV) for two-orbital Wannierization for NdNiO$_2$ and LaNiO$_2$.

i	j	k	NdNiO$_2$	LaNiO$_2$
			$t^{\text{Ni}}_{[i,j,k]}$	
0	0	0	0.306385	0.284621
1	0	0	−0.377362	−0.380994
1	1	0	0.094731	0.095830
2	0	0	−0.049510	−0.049076
0	0	1	−0.027912	−0.032524
1	0	1	−0.001615	0.000423
1	1	1	0.008920	0.009345
0	0	2	0.001415	0.000151
0	0	3	−0.000053	0.001201
			$t^{\text{Nd/La}}_{[i,j,k]}$	
0	0	0	1.493987	1.219156
1	0	0	−0.02938	−0.068788
1	1	0	−0.157513	−0.087446
2	0	0	0.051356	0.021989
0	0	1	−0.293301	−0.048961
1	0	1	0.015698	−0.196251
1	1	1	0.004019	−0.005498
0	0	2	0.027121	−0.099677
0	0	3	0.006169	−0.003715
			$t^{\text{Nd/La-Ni}}_{[i,j,k]}$	
0	0	0	0.000151	−0.011252
1	0	0	−0.000239	0.009664
1	1	0	−0.000037	0.003106
2	0	0	0.020577	0.001579
0	0	1	−0.000157	−0.006010
1	0	1	−0.007317	0.008403
1	1	1	0.000070	0.006332
0	0	2	0.000102	−0.004345
0	0	3	−0.000040	−0.001681

1. Hopping parameters for our Wannier downfolding

In consideration of the two-band model in our Hamiltonian, we chose orbital sets of Ni$_{3d_{x^2-y^2}}$ and Nd/La$_{5d_{z^2}}$ in Wannier downfolding calculations as implemented in Wannier90 [69], which can reproduce the band structure near the Fermi level accurately. The calculated hopping parameters for two-orbital Wannierization are listed in Table II.

2. The pairing symmetries of the nickel square

We referenced four kinds of pairing forms from the iron-square lattice [58], which are pictured in Fig. 7. These singlet
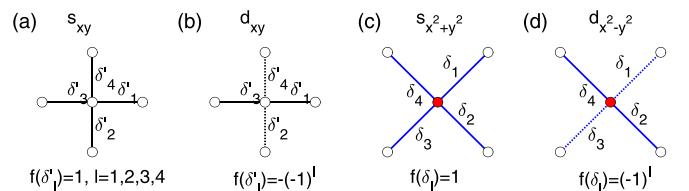

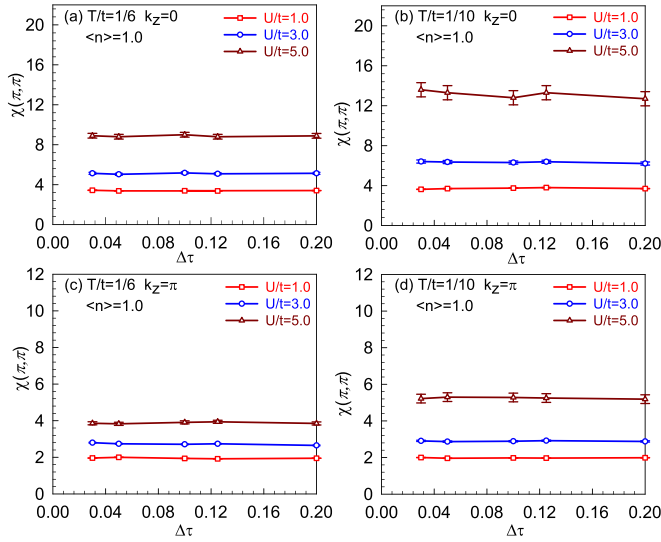FIG. 7. Phase of the s_{xy}, d_{xy}, $s_{x^2+y^2}$, and $d_{x^2-y^2}$.

FIG. 8. Influence of the imaginary time step $\Delta\tau$ to the (π, π) antiferromagnetic correlation $\chi(\pi, \pi)$ for different U at (a) $T/t = 1/6$, $k_z = 0$, (b) $T/t = 1/10$, $k_z = 0$, (c) $T/t = 1/6$, $k_z = \pi$, (d) $T/t = 1/10$, $k_z = \pi$ on a 2×8^2 lattice.

FIG. 9. Average sign $\langle \text{sign} \rangle$ as a function of nearest-neighbor interaction V for different temperatures at $\langle n \rangle = 1.0$, $U/t = 3.0$, and $k_z = 0$ on 2×12^2 or 2×8^2 lattice.

s-wave and *d*-wave pairings have the form factor

$$s_{xy}\text{-wave:} \quad f_{s_{xy}}(\delta_l') = 1, \; l = 1, 2, 3, 4,$$

$$d_{xy}\text{-wave:} \quad f_{d_{xy}}(\delta_l') = 1 \; [\delta_l' = (\pm 2\hat{x}, 0)]$$

$$\text{and} \quad f_{d_{xy}}(\delta_l') = -1 \; [\delta_l' = (0, \pm 2\hat{y})],$$

$$s_{x^2+y^2}\text{-wave:} \quad f_{s_{x^2+y^2}}(\delta_l') = 1, \; l = 1, 2, 3, 4,$$

$$d_{x^2-y^2}\text{-wave:} \quad f_{d_{x^2-y^2}}(\delta_l') = 1 \; [\delta_l' = \pm(-\hat{x}, \hat{y})]$$

$$\text{and} \quad f_{d_{x^2-y^2}}(\delta_l') = -1 \; [\delta_l' = \pm(\hat{x}, \hat{y})]. \quad \text{(A1)}$$

In experiment, by using scanning tunneling microscopy [70] or high-resolution laser ARPES [71,72], there may be a way to distinguish the d_{xy} and $d_{x^2-y^2}$ pairings.

3. Correction of the Trotter error

Since the operators H_K (kinetic energy) and H_U (potential energy) do not commute, the DQMC algorithm employs the Trotter-Suzuki decomposition to approximate the partition function and then the imaginary-time propagator can be written as

$$e^{-\Delta\tau H} \approx e^{-\Delta\tau H_K} e^{-\Delta\tau H_U}. \quad \text{(A2)}$$

In this process, we can correct systematic error by extrapolating the results at different time steps to the $\Delta\tau = 0$
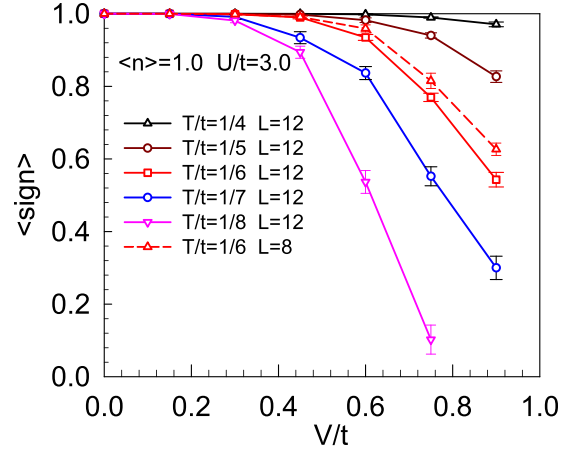
limit. In Fig. 8, we show an impact of the imaginary time step $\Delta\tau$ to the (π, π) antiferromagnetic correlation $\chi(\pi, \pi)$. The figure indicates that, regardless of the interaction strength and temperature, the $\chi(\pi, \pi)$ is essentially identical within the different time steps. Other observables can see a similar behavior. As such, Trotter errors can be negligible at the $\Delta\tau$ value used in this paper.

4. The sign problem

For the finite-temperature DQMC method, the infamous sign problem prevents accuracy of results for higher interaction, lower temperature, and larger lattice. Therefore, we assess the average of sign carefully. In our simulations, the pure on-site interaction does not make the sign-problem terrible for different electron fillings even at low temperatures (and $\langle \text{sign} \rangle \approx 1$). However, we found that the sign problem became worse when we consider the nearest-neighbor repulsion of the Ni $3d$ orbital to compute the charge density wave (CDW) state. Figure 9 shows the effect of the nearest-neighbor interaction and the temperature on the sign problem with measurements of 10 000 times. We can notice that the sign problem becomes worse with increasing interaction or decreasing temperature. Our present results are reliable because the average sign is still larger than 0.50 for $V = 0.9t$, $U/t = 3.0$, and $T/t = 1/6$ on an $L = 12$ lattice. To keep the same quality of data with $\langle \text{sign} \rangle \approx 1$, much longer measurements are essential to compensate the fluctuations. In fact, the measurements should be enlarged by a factor on the order of $\langle \text{sign} \rangle^{-2}$ [56,73]. In our simulations, we have made measurement of more than 40 000 times for some results. Therefore, the results with the current Monte Carlo parameters are reliable.

[1] J. Bardeen, L. N. Cooper, and J. R. Schrieffer, Phys. Rev. **108**, 1175 (1957).

[2] J. G. Bednorz and K. A. Müller, Z. Phys. B **64**, 189 (1986).

[3] P. W. Anderson, Science **235**, 1196 (1987).

[4] J. G. Bednorz and K. A. Müller, Rev. Mod. Phys. **60**, 585 (1988).

[5] P. W. Anderson, P. A. Lee, M. Randeria, T. M. Rice, N. Trivedi, and F. C. Zhang, J. Phys.: Condens. Matter **16**, R755 (2004).

[6] P. A. Lee, N. Nagaosa, and X.-G. Wen, Rev. Mod. Phys. **78**, 17 (2006).

[7] D. J. Scalapino, Rev. Mod. Phys. **84**, 1383 (2012).

[8] E. Fradkin, S. A. Kivelson, and J. M. Tranquada, Rev. Mod. Phys. **87**, 457 (2015).

[9] R. Comin and A. Damascelli, Annu. Rev. Condens. Matter Phys. **7**, 369 (2016).

[10] B. Keimer, S. A. Kivelson, M. R. Norman, S. Uchida, and J. Zaanen, Nature (London) **518**, 179 (2015).

[11] D. Li, K. Lee, B. Y. Wang, M. Osada, S. Crossley, H. R. Lee, Y. Cui, Y. Hikita, and H. Y. Hwang, Nature (London) **572**, 624 (2019).

[12] G. A. Sawatzky, Nature (London) **572**, 592 (2019).

[13] S. Zeng, C. S. Tang, X. Yin, C. Li, M. Li, Z. Huang, J. Hu, W. Liu, G. J. Omar, H. Jani, Z. S. Lim, K. Han, D. Wan, P. Yang, S. J. Pennycook, A. T. S. Wee, and A. Ariando, Phys. Rev. Lett. **125**, 147003 (2020).

[14] L. E. Chow, S. K. Sudheesh, P. Nandi, S. W. Zeng, Z. T. Zhang, X. M. Du, Z. S. Lim, E. E. M. Chia, and A. Ariando, arXiv:2201.10038.

[15] D. Li, B. Y. Wang, K. Lee, S. P. Harvey, M. Osada, B. H. Goodge, L. F. Kourkoutis, and H. Y. Hwang, Phys. Rev. Lett. **125**, 027001 (2020).

[16] M.-Y. Choi, K.-W. Lee, and W. E. Pickett, Phys. Rev. B **101**, 020503(R) (2020).

[17] L. Si, W. Xiao, J. Kaufmann, J. M. Tomczak, Y. Lu, Z. Zhong, and K. Held, Phys. Rev. Lett. **124**, 166402 (2020).

[18] S. Ryee, H. Yoon, T. J. Kim, M. Y. Jeong, and M. J. Han, Phys. Rev. B **101**, 064513 (2020).

[19] J. Krishna, H. LaBollita, A. O. Fumega, V. Pardo, and A. S. Botana, Phys. Rev. B **102**, 224506 (2020).

[20] M. Osada, B. Y. Wang, K. Lee, D. Li, and H. Y. Hwang, Phys. Rev. Mater. **4**, 121801(R) (2020).

[21] P. Jiang, L. Si, Z. Liao, and Z. Zhong, Phys. Rev. B **100**, 201106(R) (2019).

[22] B.-X. Wang, H. Zheng, E. Krivyakina, O. Chmaissem, P. P. Lopes, J. W. Lynn, L. C. Gallington, Y. Ren, S. Rosenkranz, J. F. Mitchell, and D. Phelan, Phys. Rev. Mater. **4**, 084409 (2020).

[23] K. Lee, B. H. Goodge, D. Li, M. Osada, B. Y. Wang, Y. Cui, L. F. Kourkoutis, and H. Y. Hwang, APL Mater. **8**, 041107 (2020).

[24] M. Osada, B. Y. Wang, B. H. Goodge, S. P. Harvey, K. H. Lee, D. F. Li, L. F. Kourkoutis, and H. Y. Hwang, Adv. Mater. **33**, 2104083 (2021).

[25] S. Zeng, C. Li, L. E. Chow, Y. Cao, Z. Zhang, C. S. Tang, X. Yin, Z. S. Lim, J. Hu, P. Yang, and A. Ariando, Sci. Adv. **8**, eabl9927 (2022).

[26] Q. Gu, Y. Li, S. Wan, H. Li, W. Guo, H. Yang, Q. Li, X. Zhu, X. Pan, Y. Nie, and H.-H. Wen, Nat. Commun. **11**, 6027 (2020).

[27] M. Zhang, Y. Zhang, H. Guo, and F. Yang, Chin. Phys. B **30**, 108204 (2021).

[28] Y.-H. Zhang and A. Vishwanath, Phys. Rev. Res. **2**, 023112 (2020).

[29] M. Kitatani, L. Si, O. Janson, R. Arita, Z. Zhong, and K. Held, npj Quantum Mater. **5**, 59 (2020).

[30] P. Adhikary, S. Bandyopadhyay, T. Das, I. Dasgupta, and T. Saha-Dasgupta, Phys. Rev. B **102**, 100501(R) (2020).

[31] X. Wu, D. Di Sante, T. Schwemmer, W. Hanke, H. Y. Hwang, S. Raghu, and R. Thomale, Phys. Rev. B **101**, 060504(R) (2020).

[32] G.-M. Zhang, Y.-f. Yang, and F.-C. Zhang, Phys. Rev. B **101**, 020501(R) (2020).

[33] C. Lu, L.-H. Hu, Y. Wang, F. Yang, and C. Wu, Phys. Rev. B **105**, 054516 (2022).

[34] H. Sakakibara, H. Usui, K. Suzuki, T. Kotani, H. Aoki, and K. Kuroki, Phys. Rev. Lett. **125**, 077003 (2020).

[35] A. Kreisel, B. M. Andersen, A. T. Rømer, I. M. Eremin, and F. Lechermann, Phys. Rev. Lett. **129**, 077002 (2022).

[36] Z. Wang, G.-M. Zhang, Y.-f. Yang, and F.-C. Zhang, Phys. Rev. B **102**, 220501(R) (2020).

[37] R. A. Ortiz, P. Puphal, M. Klett, F. Hotz, R. K. Kremer, H. Trepka, M. Hemmida, H.-A. Krug von Nidda, M. Isobe, R. Khasanov, H. Luetkens, P. Hansmann, B. Keimer, T. Schäfer, and M. Hepting, Phys. Rev. Res. **4**, 023093 (2022).

[38] H. Lu, M. Rossi, A. Nag, M. Osada, D. F. Li, K. Lee, B. Y. Wang, M. Garcia-Fernandez, S. Agrestini, Z. X. Shen, E. M. Been, B. Moritz, T. P. Devereaux, J. Zaanen, H. Y. Hwang, K.-J. Zhou, and W. S. Lee, Science **373**, 213 (2021).

[39] Y. Cui, C. Li, Q. Li, X. Zhu, Z. Hu, Y. F. Yang, J. Zhang, R. Yu, H.-H. Wen, and W. Yu, Chin. Phys. Lett. **38**, 067401 (2021).

[40] M. Rossi, M. Osada, J. Choi, S. Agrestini, D. Jost, Y. Lee, H. Lu, B. Y. Wang, K. Lee, A. Nag, Y.-D. Chuang, C.-T. Kuo, S.-J. Lee, B. Moritz, T. P. Devereaux, Z.-X. Shen, J.-S. Lee, K.-J. Zhou, H. Y. Hwang, and W.-S. Lee, Nat. Phys. **18**, 869 (2022).

[41] C. C. Tam, J. Choi, X. Ding, S. Agrestini, A. Nag, M. Wu, B. Huang, H. Luo, P. Gao, M. García-Fernández, L. Qiao, and K.-J. Zhou, Nat. Mater. **21**, 1116 (2022).

[42] G. Krieger, L. Martinelli, S. Zeng, L. E. Chow, K. Kummer, R. Arpaia, M. Moretti Sala, N. B. Brookes, A. Ariando, N. Viart, M. Salluzzo, G. Ghiringhelli, and D. Preziosi, Phys. Rev. Lett. **129**, 027002 (2022).

[43] C. Peng, H.-C. Jiang, B. Moritz, T. P. Devereaux, and C. Jia, arXiv:2110.07593.

[44] H. Chen, Y. F. Yang, and G.-M. Zhang, arXiv:2204.12208.

[45] Y. Shen, M. Qin, and G.-M. Zhang, arXiv:2207.00266.

[46] V. I. Anisimov, D. Bukhvalov, and T. M. Rice, Phys. Rev. B **59**, 7901 (1999).

[47] K.-W. Lee and W. E. Pickett, Phys. Rev. B **70**, 165109 (2004).

[48] A. S. Botana and M. R. Norman, Phys. Rev. X **10**, 011024 (2020).

[49] E. Been, W.-S. Lee, H. Y. Hwang, Y. Cui, J. Zaanen, T. Devereaux, B. Moritz, and C. Jia, Phys. Rev. X **11**, 011050 (2021).

[50] M. Hepting, D. Li, C. J. Jia, H. Lu, E. Paris, Y. Tseng, X. Feng, M. Osada, E. Been, Y. Hikita, Y.-D. Chuang, Z. Hussain, K. J. Zhou, A. Nag, M. Garcia-Fernandez, M. Rossi, H. Y. Huang, D. J. Huang, Z. X. Shen, T. Schmitt *et al.*, Nat. Mater. **19**, 381 (2020).

[51] M. Jiang, M. Berciu, and G. A. Sawatzky, Phys. Rev. Lett. **124**, 207004 (2020).

[52] Y. Nomura, M. Hirayama, T. Tadano, Y. Yoshimoto, K. Nakamura, and R. Arita, Phys. Rev. B **100**, 205138 (2019).

[53] L.-H. Hu and C. Wu, Phys. Rev. Res. **1**, 032046(R) (2019).

[54] J. Karp, A. S. Botana, M. R. Norman, H. Park, M. Zingl, and A. Millis, Phys. Rev. X **10**, 021061 (2020).

[55] F. Lechermann, Phys. Rev. X **10**, 041002 (2020).

[56] R. Blankenbecler, D. J. Scalapino, and R. L. Sugar, Phys. Rev. D **24**, 2278 (1981).

[57] T. Ma, F. Hu, Z. Huang, and H.-Q. Lin, Appl. Phys. Lett. **97**, 112504 (2010).

[58] T. Ma, H.-Q. Lin, and J. Hu, Phys. Rev. Lett. **110**, 107002 (2013).

[59] S. R. White, D. J. Scalapino, R. L. Sugar, E. Y. Loh, J. E. Gubernatis, and R. T. Scalettar, Phys. Rev. B **40**, 506 (1989).

[60] L. Wang, P. Corboz, and M. Troyer, New J. Phys. **16**, 103008 (2014).

[61] Z.-X. Li, Y.-F. Jiang, and H. Yao, Phys. Rev. B **91**, 241117(R) (2015).

[62] Y.-X. Zhang, W.-T. Chiu, N. C. Costa, G. G. Batrouni, and R. T. Scalettar, Phys. Rev. Lett. **122**, 077602 (2019).

[63] J. Karp, A. Hampel, and A. J. Millis, Phys. Rev. B **105**, 205131 (2022).

[64] M. Klett, P. Hansmann, and T. Schäfer, Front. Phys. **10**, 834682 (2022).

[65] S. P. Harvey, B. Y. Wang, J. Fowlie, M. Osada, K. Lee, Y. Lee, D. Li, and H. Y. Hwang, arXiv:2201.12971.

[66] M. Hayward and M. Rosseinsky, Solid State Sci **5**, 839 (2003).

[67] X. Sui, J. Wang, X. Ding, K.-J. Zhou, L. Qiao, H. Lin, and B. Huang, arXiv:2202.11904.

[68] C. Chen, R. Ma, X. Sui, Y. Liang, B. Huang, and T. Ma (unpublished).

[69] A. A. Mostofi, J. R. Yates, Y.-S. Lee, I. Souza, D. Vanderbilt, and N. Marzari, Comput. Phys. Commun **178**, 685 (2008).

[70] P. O. Sprau, A. Kostin, A. Kreisel, A. E. Böhmer, V. Taufour, P. C. Canfield, S. Mukherjee, P. J. Hirschfeld, B. M. Andersen, and J. C. S. Davis, Science **357**, 75 (2017).

[71] B. Béri, J. N. Kupferschmidt, C. W. J. Beenakker, and P. W. Brouwer, Phys. Rev. B **79**, 024517 (2009).

[72] P. Ai, Q. Gao, J. Liu, Y. Zhang, C. Li, J. Huang, C. Song, H. Yan, L. Zhao, G.-D. Liu, G.-D. Gu, F.-F. Zhang, F. Yang, Q.-J. Peng, Z.-Y. Xu, and X.-J. Zhou, Chin. Phys. Lett. **36**, 067402 (2019).

[73] R. R. d. Santos, Braz. J. Phys. **33**, 36 (2003).